Prognosis using Bayesian Method by Incorporating Physical Constraints

Hyung Jun Park[1], Nam H. Kim[2], and Joo-Ho Choi[3]

[1] *Dept. of Aerospace & Mechanical Engineering, Korea Aerospace University, Goyang-si, Gyeonggi-do, 10540, Korea*
phj921029@kau.kr

[2]*Dept. of Mechanical and Aerospace Engineering, University of Florida, Gainesville, Florida, FL 32611, USA*
nkim@ufl.edu

[3]*School. of Aerospace & Mechanical Engineering, Korea Aerospace University, Goyang-si, Gyeonggi-do, 10540, Korea*
jhchoi@kau.ac.kr

ABSTRACT

Accurately predicting the remaining useful life (RUL) of industrial machinery is crucial for ensuring their reliability and safety. Prognostic methods that rely on Bayesian inference, such as Bayesian method (BM), Kalman and Particle filter (KF, PF), have been extensively studied for the RUL prognosis. However, these algorithms can be affected by noise when training data is limited, and the uncertainty associated with empirical models that are used in place of expensive physics models. As a result, this can lead to significant prediction errors or even infeasible RUL prediction in some cases. To overcome this challenge, three different approaches are proposed to guide the Bayesian framework by incorporating low-fidelity physical information. The proposed approaches embed inequality constraints to reduce sensitivity to local observations and achieve robust prediction. To determine an appropriate approach and its advantageous features, performance is evaluated by both numerical example and real case study for drone motor degradation.

1. INTRODUCTION

The prognostic algorithms for RUL prediction are generally divided into two categories: data-driven and model-based approaches (Kim et al., 2021a; Sutharssan et al., 2015). Data-driven approaches use historical datasets to identify degradation patterns using artificial intelligence (AI) methods but require a huge amount of training data. Insufficient training data may lead to poor accuracy and large training uncertainty to make proper decision-making. In contrast, model-based approaches use physical model that describes the machinery degradation behavior and enables more accurate and long-term prediction. Bayesian inference-based prognostic algorithms such as Bayesian method (BM) (An et al., 2012), Kalman filter (KF) (Lim and Mba, 2015) and Particle filter (PF) (Kim et al., 2021b) are commonly used to estimate the model parameters.

In practice, however, it is challenging to establish high-fidelity physics model for complex machinery system as the degradation process can involve various components and failure mechanisms. As an alternative, simple but effective mathematical models such as a single exponential model (Kim et al., 2022b; Wang et al., 2021), polynomial model (Kim et al., 2017) or dual-exponential model (Chen et al., 2020) are widely used in model-based approaches. However, traditional Bayesian inference-based algorithms present several challenges when used with these models, leading to inaccurate predictions of RUL. The first issue is that the simple mathematical models used may not be able to accurately capture the complexities of non-linear degradation processes, resulting in significant prediction errors. Additionally, inaccurate, or insufficient measurements can produce unexpected results and increase prediction uncertainty. Our research has revealed that these challenges have not been thoroughly addressed in existing prognostic algorithms that use traditional Bayesian frameworks.

To address above issues, we have developed three approaches that incorporate physical constraints into conventional Bayesian methods. These approaches aim to reduce the sensitivity of prognostic algorithms to local, noisy measurements and improve RUL prediction accuracy, particularly in the early stages of degradation. Moreover, we have also included multiple noise perturbations at the same noise level in our simulated degradation model to properly quantify prediction uncertainty.

2. BAYESIAN METHOD

In Bayes' theorem, the knowledge of a system can be improved with additional observation of the system. In BM,

the joint posterior PDF of degradation model parameters at the current time is obtained by a single equation, in which all the likelihood of measured data are multiplied. More specifically, let $\boldsymbol{\theta}$ be the vector of unknown model parameters and $\boldsymbol{y}_{1:k}$ is the vector of observed data until time k. The joint posterior PDF is obtained by multiplying the prior PDF with the likelihood as

$$p(\boldsymbol{\theta}|\boldsymbol{y}_{1:k}) \propto= p(\boldsymbol{y}_{1:k}|\boldsymbol{\theta})p(\boldsymbol{\theta}) \quad (1)$$

$$p(\boldsymbol{y}_{1:k}|\boldsymbol{\theta}) = (\sigma^2)^{-k/2} exp\left\{-\frac{1}{2\sigma^2}(\boldsymbol{y}_{1:k} - \hat{\boldsymbol{y}}_{1:k})^T(\boldsymbol{y}_{1:k} - \hat{\boldsymbol{y}}_{1:k})\right\} \quad (2)$$

where $p(\boldsymbol{\theta})$ is the prior PDF of parameters, $p(\boldsymbol{y}_{1:k}|\boldsymbol{\theta})$ is the multiplied likelihood of observed data conditional on the given parameter value $\boldsymbol{\theta}$ as Eq. (2) where $\hat{\boldsymbol{y}}_{1:k}$ is the model prediction.

After obtaining the expression of posterior PDF by Eq. (1), N samples of parameters are drawn using a sampling method, with the Markov-chain Monte Carlo (MCMC) algorithm being used in this study due to its effectiveness in producing complex posterior distributions. Fig. 1 shows the sampling process using the Metropolis-Hasting (M-H) algorithm, which is a typical MCMC method. Initial settings such as the initial value for parameters $\boldsymbol{\theta_0}$, the initial prior distribution $p(\boldsymbol{\theta})$ and the weight vector $\boldsymbol{w}$ for the sampling interval of the proposal distribution $g(\boldsymbol{\theta}^*|\boldsymbol{\theta}^{i-1})$ which is the uniform distribution are set by the user. A new sample $\boldsymbol{\theta}^*$ is drawn from the proposal distribution and the selection is proceeded based on the acceptance criterion as

$$Q(\boldsymbol{\theta}^{i-1}, \boldsymbol{\theta}^*) = \boldsymbol{min}\left\{1, \frac{p(\boldsymbol{\theta}^*|\boldsymbol{y})}{p(\boldsymbol{\theta}^{i-1}|\boldsymbol{y})}\right\} \quad (3)$$

where proposal distribution is removed since it is a symmetric distribution. The new sample is accepted if its PDF value is greater than the old sample's. Otherwise, acceptance depends on the ratio of PDF values and a random sample u. With sufficient iterations, the sampling results approximate the posterior distribution. More detailed explanations are given in (An et al., 2010; Andrieu and Jordan, 2003; Kim Dawn An Joo-Ho Choi, n.d.).

BM process

- **Initial settings**

: Set initial value $\boldsymbol{\theta_0}$, initial prior distribution $p(\boldsymbol{\theta})$, weight $\boldsymbol{w}$

- **MH algorithm**

: For $i = 1, \dots, N$

- Generate new sample from proposal distribution

  $\boldsymbol{\theta}^* \sim g(\boldsymbol{\theta}^*|\boldsymbol{\theta}^{i-1}) = U(\boldsymbol{\theta}^{i-1} - \boldsymbol{w}, \boldsymbol{\theta}^{i-1} + \boldsymbol{w})$

- Generate acceptance sample $u \sim U(0,1)$

- If $u < Q(\boldsymbol{\theta}^{i-1}, \boldsymbol{\theta}^*)$

  $\boldsymbol{\theta}^i = \boldsymbol{\theta}^*$

  Else

  $\boldsymbol{\theta}^i = \boldsymbol{\theta}^{i-1}$

Figure 1. Process of Bayesian method.

2.1. Physical constraints

This study utilizes the low-fidelity physical information to impose physical constraints in the prognostic algorithms outlined in previous sections. Low-fidelity physical information refers to the lowest level of physical information available, which crudely represents parameter behavior during degradation (Kim et al., 2022a). To clarify, physical constraints are exemplified through a polynomial degradation model, which will be discussed in detail in the numerical study:

$$x_k = C + \beta_1 {t_k}^2 + \beta_2 {t_k}^3 \quad (4)$$

where $\boldsymbol{\beta} = [\beta_1, \beta_2]$ is model parameters, C is constant initial value and t_k is time/cycles. In case of degradation, it is widely known that the damage state x_k should inherently increase over time (i.e. $dx/dt \geq 0$) and the slope of degradation is a positive trend (i.e. a non-linearly increasing trend, $dx^2/dt^2 \geq 0$). This two information is defined as monotonicity (Mon) and curvature (Cur), respectively. In the Section 3, the methods to utilize the two physical constraints in the prognostic algorithms following the Bayesian inference are addressed.

3. METHODOLOGY

This section outlines our methodology for incorporating physical constraints into the BM algorithm to facilitate robust prognosis in the face of severe noise and limited data (i.e. early prediction). As depicted in Fig. 2, three distinct encoding methods are proposed to guide the prognostic algorithms with physical constraints. Additionally, we introduce a prognosis performance metric that quantifies data uncertainty resulting from random noise.

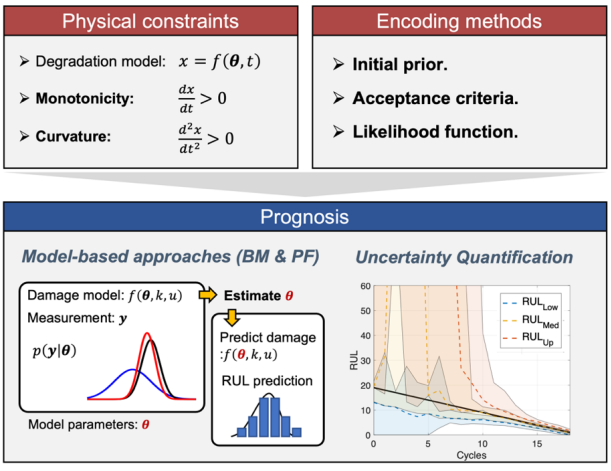

Figure 2. The proposed methodology for prognostics guided by physical constraints.

3.1. Method 1: initial prior constraints

A simple and direct approach to embed constraints in Bayesian updating is to set the boundaries of the initial prior

distribution. Specifically, with the polynomial damage model, there may be several inequality constraints ($a_j \le \beta_j \le b_j, \quad j = 1,2$) on the true model parameters $\boldsymbol{\beta_{true}}$. In BM, the initial prior distribution is assumed to be uniform and will be truncated according to the boundaries, which will impact the resulting posterior distribution. The constrained posterior PDF $p_c(\boldsymbol{\theta}|\boldsymbol{y}_{1:k})$ is expressed as Eq. (5) and will sample from truncated $Q_c(\boldsymbol{\theta}^{i-1}, \boldsymbol{\theta}^*)$.

$$p_c(\boldsymbol{\theta}|\boldsymbol{y}_{1:k}) \propto p(\boldsymbol{y}_{1:k}|\boldsymbol{\theta}) p_c(\boldsymbol{\theta}) \text{ where } p_c(\theta_j) \sim U(a_j, b_j) \quad (5)$$

The detailed information about obtaining the prior boundaries $[\boldsymbol{a}, \boldsymbol{b}]$ is addressed in numerical case study.

3.2. Method 2: acceptance criteria constraints

To embed physical constraints in Bayesian updating, another approach involves setting additional acceptance criteria for new samples generated from the proposal distribution. This is done by calculating the Mon and Cur values of the new sample not just within the interpolation region but also in the extrapolation region. Parameters that do not result in a monotonic increase in degradation in the extrapolation region are eliminated.

The process is explained via Fig. 3. As shown in the figure, the new model parameter samples $\boldsymbol{\beta}^* = [\boldsymbol{\beta}_1^*, \boldsymbol{\beta}_2^*]$ at 9 cycles are obtained with measurements using BM, in which the future state and uncertainty is predicted to prediction points T_p by red lines. The T_p include both the interpolation and extrapolation regions and should be defined in prior with sufficient prediction range. Then, the vectors of Mon ($\hat{\boldsymbol{y}}_{\boldsymbol{m}}$) and Cur ($\hat{\boldsymbol{y}}_{\boldsymbol{c}}$) of predicted health state are calculated with a vector of cycles from initial point to the prediction points as

$$\begin{cases} \hat{\boldsymbol{y}}_{\boldsymbol{m}} = dx/dt \ = 2\boldsymbol{\beta}_1^* \boldsymbol{t}_{T_p} + 3\boldsymbol{\beta}_2^* \boldsymbol{t}_{T_p}^2 \\ \hat{\boldsymbol{y}}_{\boldsymbol{c}} = dx^2/dt^2 \ = 2\boldsymbol{\beta}_1^* + 6\boldsymbol{\beta}_2^* \boldsymbol{t}_{T_p} \end{cases} \text{ where } \boldsymbol{t}_{T_p} = [1,2,\dots,T_p] \quad (6)$$

The new sample is accepted not only based on the ratio of PDF values but also when both $\hat{\boldsymbol{y}}_{\boldsymbol{m}}$ and $\hat{\boldsymbol{y}}_{\boldsymbol{c}}$ are positive ($\hat{\boldsymbol{y}}_{\boldsymbol{m}} \ge \boldsymbol{0}$ & $\hat{\boldsymbol{y}}_{\boldsymbol{c}} \ge \boldsymbol{0}$).

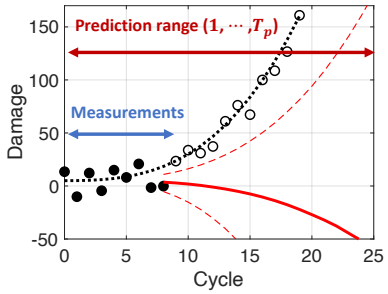

Figure 3. Constraint calculation with prediction points

3.3. Method 3: likelihood function constraints

Finally, in method 3, the physical constraints are imposed in the form of penalties in the cost function, i.e. likelihood function. Similarly, the physical constraint term is violated whenever the monotonicity and the curvature are negative. In this method, the estimation process of prognostic algorithms is interpreted as a constrained optimization problem as shown in the below form:

$$\begin{aligned} &\text{Minimize} \quad MSE = \sum_{i=1}^{N} (y_i - \hat{y}_i)^2 \\ &\text{Subject to} \quad \sum_{k=1}^{T_p} max[0, -\hat{y}_{m,k}] < 0 \ \& \ \sum_{k=1}^{T_p} max[0, -\hat{y}_{c,k}] < 0 \end{aligned} \quad (7)$$

To solve the inequality constrained optimization problem, the constrained optimization formulation can be approximated into an unconstrained problem by using a Lagrange multiplier method. As a result, Eq. (7) is converted into the following cost function:

$$\begin{aligned} cost &= MSE + \lambda_1 \sum_{k=1}^{T_p} max[0, -\hat{y}_{m,k}] + \lambda_2 \sum_{k=1}^{T_p} max[0, -\hat{y}_{c,k}] \\ &= MSE + \lambda_1 penalty_1 + \lambda_2 penalty_2 \end{aligned} \quad (8)$$

where λ_1 and λ_2 are the Lagrange multiplier for the physical constraints penalties. The form of Eq. (8) can be embedded in calculation of the likelihood for BM as addressed in the following equation:

$$p_{c,BM}(y|\theta^*) = \left(\sigma\sqrt{2\pi}\right)^{-k} exp\left[-\left(\frac{1}{2\sigma^2}(y-\hat{y})^T(y-\hat{y}_k) + \lambda_1 penalty_1 + \lambda_2 penalty_2\right)\right] \quad (9)$$

The physical constraint acts as a role of a regularization term and reduces the complexity of the degradation model due to overfitting to noisy data. In result, the physical constraint term prevents overfitting from local noisy data and ensures reasonable prediction based on physical knowledge.

4. PROGNOSIS PERFORMANCE METRICS

4.1. Prediction accuracy

The average RUL prediction accuracy from the noise randomness is evaluated by mean absolute error (MAE) defined as (Son et al., 2016)

$$MAE_k = \frac{1}{M} \sum_{i=1}^{M} \left| \widehat{RUL}_m(\boldsymbol{\theta_k}) - RUL_{True}(\boldsymbol{\theta_k}) \right| \quad (10)$$

where $\widehat{RUL}_m$ represents the median value of predicted RUL by estimated model parameters using measured data until time k, and RUL_{True} is true RUL value. In addition, the performance of the prognostic algorithm depends not only on the level of random noise, but also the amount of measured data for model parameter estimation. Thus, the performance comparison with the physical constrained BM will be conducted under different time cycle k to predict RUL.

4.2. Prediction uncertainty

From the perspective of decision makers, in addition to prediction error, it is important to quantify the uncertainty of the prediction and it can be assessed by the C.I. of the RUL prediction (Gebraeel N et al., 2023). However, owing to noise randomness, the uncertainty bound can also have uncertainty

due to noise randomness. To quantify algorithm consistency, RUL predictions for M datasets are stored in a table shown in Fig. 4, and the 90% C.I. and median are calculated. RUL curve uncertainty is represented with a shaded surface in Fig. 4. This approach was studied in the previous study by the authors (Kim et al., 2022a).

Dataset	Percentile		
	5%	50%	95%
Data 1	$\widehat{RUL}_L$	$\widehat{RUL}_M$	$\widehat{RUL}_U$
Data 2	$\widehat{RUL}_L$	$\widehat{RUL}_M$	$\widehat{RUL}_U$
⋮	⋮	⋮	⋮
Data M	$\widehat{RUL}_L$	$\widehat{RUL}_M$	$\widehat{RUL}_U$

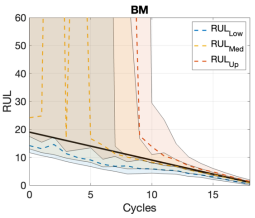

Figure 4. Data uncertainty quantification in RUL curve

5. NUMERICAL STUDY

In this section, the proposed methods are applied via a simulation data of non-linear degradation, in which the Eq. (4) with the model parameter $\boldsymbol{\beta}$ is used to create degradation data added by random noise ϵ that follows Gaussian distribution with standard deviation σ:

$$x_k = C + \beta_1 {t_k}^2 + \beta_2 {t_k}^3 \text{ and } y_k = x_k + \epsilon \text{ with } \epsilon \sim N(0, \sigma) \quad (11)$$

where true value of $\boldsymbol{\beta_1}$ and $\boldsymbol{\beta_2}$ is 0.05 and 0.02, respectively. To consider moderate and severe noisy condition, the σ value is set 10 or 50. Moreover, in this study, 50 datasets are generated with random noise to compare prediction performance between general Bayesian framework and our proposed method.

5.1. Prediction results

To apply physical constraints by method 1, first, we need to obtain the range of initial prior distribution range for the parameters. Unlike the most of related studies that provide prior constraints by expert knowledge, this paper identifies the prior constraint range by the combination of monotonicity and curvature grid. To obtain grid, a sufficient range that cover true parameter value is set in prior. In this study, it is set between -0.1 to 0.1 for both β_1 and β_2. Then at each cycle, the Mon and Cur values are calculated over the grid and define as 1 if only both Mon and Cur are positive, otherwise as 0. The Fig. 5 shows the result over initial cycle to prediction point T_p which is set 50 cycles in this study. Finally, the overlapping area over cycles is used for constraint prior range as

$$f(\beta_1) \sim U(0,\ 0.1)\ \&\ f(\beta_2) \sim U(0,\ 0.1)$$

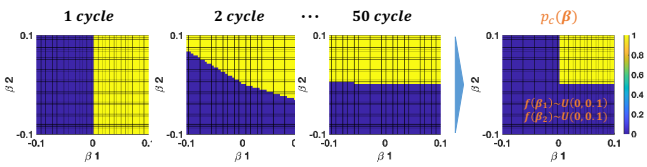

Figure 5. Initial constraint prior range calculation

BM and the proposed constraint methods were used to predict future degradation based on data up to 9 cycles, as shown in Fig. 6(a) and (b) for datasets with varying levels of noise. The red dotted and dashed lines refer to predicted 90% C.I. and median using black dotted data. The original BM performed poorly due to inaccurate estimation of the posterior state caused by the noisy data, resulting in violation of the monotonicity principle and a decreasing trend in time for the median of the predicted distribution. In contrast, the proposed methods produced satisfactory predictions with a median of the predicted distribution that is both monotonically increasing and close to the true degradation, with reduced uncertainty.

Even in the large noise dataset, the proposed methods shows great performance compared to the original BM without constraints. Thus, constraining the conventional Bayesian framework with physical constraints avoids large prediction errors caused by local noisy data and predicts the degradation trajectory monotonically even under large noise condition. Even if the median prediction from the large noise level seems more accurate than that of the small noise level, this is by accident due to the realization of noise.

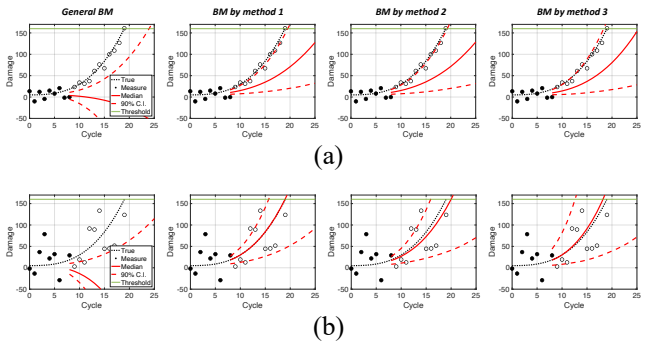

(a)

(b)

Figure 6. Prediction using BM and proposed methods: (a) under small-level of noise (b) large-level of noise

5.2. Prediction performance analysis

In this section, the two metrics are used to compare prediction performance of conventional BM with our proposed methods. Fig. 7 shows the MAE of 50 random datasets at different cycles. The column shows the MAE by the prediction from initial 5 cycles to 15 cycles, and the row represents the different noise levels and methods. The results show that our proposed method has a greater performance compared to the original BM, especially in the earlier stage (5~9 cycles). However, as more measurements are used until later stages (15 cycles), the prediction accuracies for both BM and constrained BM show not much difference. The grey shaded column represents the sum of MAEs from 5 to 15 cycles, and our proposed method has a reduced MAE of about 17 times compared to the original BM. Moreover, under the large noise data, the constrained methods show higher performance in the later stage.

	Method	MAE					
		5 cycle	⋯	*9 cycle*	⋯	*15 cycle*	*Overall (1 ~ 20)*
$\sigma = 10$	BM	172.89	⋯	21.35	⋯	0.61	949.76
	BM by method 1	3.57	⋯	2.85	⋯	0.63	54.98
	BM by method 2	3.84	⋯	2.56	⋯	0.63	56.28
	BM by method 3	3.92	⋯	2.60	⋯	0.65	57.24
$\sigma = 50$	BM	155.15	⋯	102.02	⋯	9.35	1445.99
	BM by method 1	3.98	⋯	3.97	⋯	2.39	85.25
	BM by method 2	4.03	⋯	3.73	⋯	2.41	74.86
	BM by method 3	4.21	⋯	4.05	⋯	2.12	72.55

Figure 7. MAE of 50 random datasets by BM

Fig. 8 shows RUL curve plots with data uncertainty using the original BM and proposed methods. Fig. 8(a) presents the results under small noise level. The black line represents the true RUL value, while the red dashed line and shaded area represent the median and 90 C.I. of predicted RUL upper bound, respectively. The yellow and blue lines indicate the predicted RUL median and lower bound. The proposed constrained methods show reduced uncertainty and high accuracy compared to the general BM, particularly in the earlier stages. In the case of large noise data, the general BM fails to provide robust prediction. However, the proposed methods offer consistent uncertainty and accurate prediction of median throughout the stages.

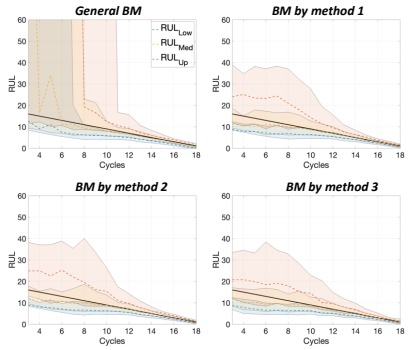

(a)

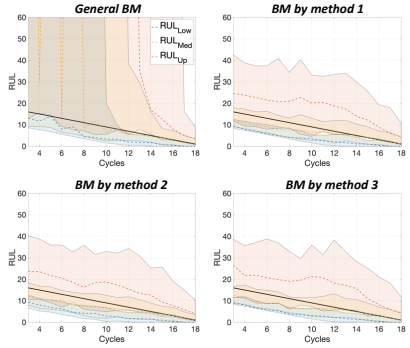

(b)

Figure 8. RUL curve plot using BM with (a) small noise level (b) large noise level

In the following real case study, method 1 has difficulty obtaining the prior distribution knowledge in high dimensions and method 2 has the potential to discard samples that do not have a low likelihood. Thus, method 3 is implemented since it has the advantage of regularization effect without risk of losing samples, but the values of penalty parameters need to be selected appropriately. The computational complexity of each method is similar.

6. CASE STUDY

The Parrot Mambo drone (PMD) equipped with an 8520 coreless DC motor is used as a real case study for RUL prognosis (Susini, n.d.). The PMD undergoes an accelerated test by taking off and hovering at 1.1m altitude with intermittent intervals. After 106 hours of experiment (48 cycles of hovering tests), motor 4 experiences degradation. A health indicator (HI) of the motors, maximum thrusts, is estimated using Kalman filter (KF) at each cycle. In Fig. 9, the HI results for motor 1 (normal) and motor 4 (degraded) are shown as blue dots and red filled dots, respectively. Motor 1 maintains its value between 0.2434 to 0.2370, while motor 4 nonlinearly decreases and reaches the threshold (magenta-colored line). RUL prediction is performed using these measurements with BM by constraint method 3.

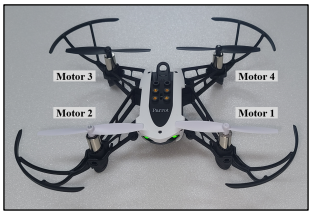

(a)

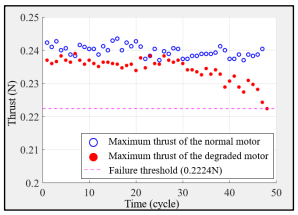

(b)

Figure 9. (a) PMD (b) HI of motor at each cycle

6.1. Prediction results

Empirical degradation model for the motor HI is defined by the dual exponential function in terms of cycles, as it is widely employed for the non-linearly degrading trend such as batteries (He et al., 2011; Xing et al., 2013).

$$x_k = \beta_{1,k} exp\left(\beta_{2,k} t_k\right) + \beta_{3,k} exp\left(\beta_{4,k} t_k\right) \quad (12)$$

where x_k is the HI of the motor, t_k is the cycle index, and $\beta_i (i = 1, \ldots, 4)$ are the model parameters. Initial prior distribution of the parameters to implement BM procedure are assumed as follows, which is rough range based on the degradation fitting over the entire cycles. From these, 5000 samples are generated to be used for the sampling in BM.

$$x_0 \sim U(0.23, 0.25),\ \beta_2 \sim U(0.05, 0.15),\ \beta_3 \sim U(0.2, 0.4)$$
$$\beta_{1,4} \sim U(-0.05, 0.05),\ \sigma \sim U(0, 0.1)$$

Fig. 10(a) and (b) compare the RUL prediction performance of different methods. Fig. 10(a) shows the comparison between the general BM and BM with constraint method. The red and blue dashed lines represent the prediction median of

the general BM and BM with constraint, respectively. The dotted line represents the prediction interval (P.I.) with estimated noise. The results show that the constrained BM gives more accurate and realistic prediction with narrower uncertainty bound compared to the general BM.

Fig. 10(b) compares the RUL prediction under a single exponential model, a dual exponential model, and a dual exponential model with constraint method 3. The yellow shaded area represents the predicted RUL with 90% P.I. under the single exponential model from 20 cycles. The two parallel black dotted lines indicate an allowable error bound (α %) around the true RUL, set to 10% in this study. The blue and red stars represent the first cycle index when the predictions reside in the accuracy zone. The red shaded area represents the predicted RUL under the dual exponential model and resides in the allowable error bound after about 34 cycles. However, the original BM suffers from large fluctuations in the earlier stages and cannot provide reliable predictions over cycles. In contrast, the blue shaded area by the proposed constrained BM method shows reliable and accurate RUL prediction from 23 cycles, which is 11 cycles earlier than the original BM.

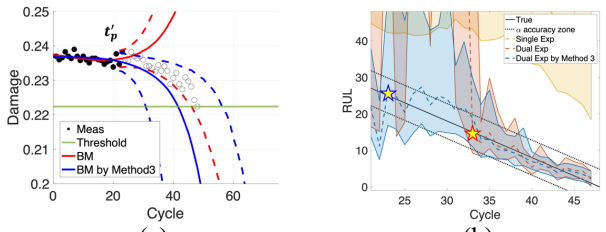

(a) (b)

Figure 10. Plot of (a) BM and BM by method 3 (b) RUL curve comparison by BM

7. CONCLUSION

The study proposed three approaches to improve the Bayesian framework for degradation prediction by incorporating low-fidelity physical information and inequality constraints. The proposed methods effectively reduced uncertainty and achieved better results, even with large noise in the dataset. Future work will integrate other Bayesian-based prognosis algorithms with physical constraints and study the optimal Lagrange multiplier value for regularization. In addition, implementing constraints with more complex physical equations will be further investigated.

ACKNOWLEDGEMENT

This research was supported by the MOTIE (Ministry of Trade, Industry, and Energy) in Korea, under the Fostering Global Talents for Innovative Growth Program (P0017307) supervised by the Korea Institute for Advancement of Technology (KIAT).

REFERENCES

An, D., Choi, J.H., Kim, N.H., (2012). Identification of correlated damage parameters under noise and bias using Bayesian inference. *Struct Health Monit* 11, 293–303.

An, D. W., Gang, J. H., Choi, J. H. (2010). MCMC Approach for Parameter Estimation in the Structural Analysis and Prognosis. *Journal of the Computational Structural Engineering Institute of Korea*, 23(6), 641-649.

Andrieu, C., Jordan, M.I., (2003). An Introduction to MCMC for Machine Learning.

Chen, Y., He, Y., Li, Z., Chen, L., Zhang, C., (2020). Remaining useful life prediction and state of health diagnosis of lithium-ion battery based on second-order central difference particle filter. *IEEE Access* 8, 37305–37313.

He, W., Williard, N., Osterman, M., Pecht, M., (2011). Prognostics of lithium-ion batteries based on Dempster-Shafer theory and the Bayesian Monte Carlo method. *Journal of Power Sources* 196, 10314–10321.

Gebraeel, N., Lei, Y., Li, N., Si, X., Zio, E., (2023). Prognostics and Remaining Useful Life Prediction of Machinery: Advances, Opportunities and Challenges. *Journal of Dynamics, Monitoring and Diagnostics*.

Kim, N. H., An, D., & Choi, J. H. (2017). Prognostics and health management of engineering systems. Switzerland: *Springer International Publishing*.

Kim, S., Choi, J.H., Kim, N.H., (2022a.) Data-driven prognostics with low-fidelity physical information for digital twin: physics-informed neural network. *Structural and Multidisciplinary Optimization* 65.

Kim, S., Kim, N.H., Choi, J.H., (2021a). A Study Toward Appropriate Architecture of System-Level Prognostics: Physics-Based and Data-Driven Approaches. *IEEE Access* 9, 157960–157972.

Kim, S., Park, H.J., Choi, J.H., Kwon, D., (2021b). A Novel Prognostics Approach Using Shifting Kernel Particle Filter of Li-Ion Batteries under State Changes. *IEEE Transactions on Industrial Electronics* 68, 3485–3493.

Kim, S., Park, H.J., Seo, Y.H., Choi, J.H., (2022b). A Robust Health Indicator for Rotating Machinery under Time-Varying Operating Conditions. *IEEE Access* 10, 4993–5001.

Lim, C.K.R., Mba, D., (2015). Switching Kalman filter for failure prognostic. *Mech Syst Signal Process* 52–53, 426–435.

Son, J., Zhou, S., Sankavaram, C., Du, X., Zhang, Y., (2016). Remaining useful life prediction based on noisy condition monitoring signals using constrained Kalman filter. *Reliab Eng Syst Saf* 152, 38–50.

Susini, A., n.d. RIMMA Risk Information Management, Risk Models, and Applications.

Sutharssan, T., Stoyanov, S., Bailey, C., Yin, C., (2015). Prognostic and health management for engineering systems: a review of the data-driven approach and algorithms. *The Journal of Engineering*, 215–222.

Wang, Q., Xu, K., Kong, X., Huai, T., (2021). A linear mapping method for predicting accurately the RUL of rolling bearing. *Measurement* (Lond) 176.

Xing, Y., Ma, E.W.M., Tsui, K.L., Pecht, M., (2013). An ensemble model for predicting the remaining useful performance of lithium-ion batteries. *Microelectronics Reliability* 53, 811–820.